Astrophysical reaction rate for ^{17}F(p,γ)^{18}Ne from the transfer reaction ^{13}C(^{17}O,^{18}O)^{12}C

T. Al-Abdullah,[1,2,*] F. Carstoiu,[3] X. Chen,[1,†] H. L. Clark,[1] C. A. Gagliardi,[1] Y.-W. Lui,[1] A. Mukhamedzhanov,[1] G. Tabacaru,[1] Y. Tokimoto,[1] L. Trache,[1,3] R. E. Tribble,[1] and Y. Zhai[1,‡]

[1]*Cyclotron Institute, Texas A&M University, College Station, Texas 77843-3366, USA*
[2]*Physics Department, The Hashemite University, Zarqa 13115, Jordan*
[3]*National Institute for Physics and Nuclear Engineering Horia Hulubei, Bucharest, Romania*

The asymptotic normalization coefficients of the bound states $J^\pi = (0_1^+, 2_1^+, 4_1^+, 2_2^+)$ in ^{18}O are extracted from the peripheral neutron transfer reaction ^{13}C(^{17}O,^{18}O)^{12}C. They are then converted to their mirror states in ^{18}Ne, which are further used to evaluate the astrophysical S factor for the proton capture reaction ^{17}F(p,γ)^{18}Ne. The elastic-scattering cross sections have been measured in both incoming and outgoing channels in order to extract the optical potentials needed for distorted-wave-Born-approximation calculations. The S factor is found to be $S_{1-17}(0) = 2.17 \pm 0.37$ keV b. The contribution of the direct capture rate to this reaction is estimated, and its consequences on the production of ^{18}F at stellar energies in ONe novae are discussed.

PACS number(s): 21.10.Jx, 26.30.−k, 25.70.Hi, 27.30.+t

I. INTRODUCTION

Nucleosynthesis of elements in ONe white dwarf (WD) novae produces several sources of γ-ray lines. Among them is the positron-electron annihilation in the nova envelope, which leads to a strong line at 511 keV and a continuum below it. It is believed that ^{13}N ($t_{1/2} = 9.965$ min) and ^{18}F ($t_{1/2} = 109.77$ min) are the main contributors to the production of observable positron annihilation radiation [1]. Because of the short lifetime of ^{13}N, the decay of ^{18}F is more important since its γ-ray photons are emitted when the envelope starts to be transparent [1–3]. According to the ONe novae models, when the temperature in the burning shell reaches $T_9 \sim 0.2$–0.4, the main nuclear activity to produce ^{18}F is driven by a β decay following the proton capture reaction ^{17}F(p,γ)^{18}Ne [4]. This is an important reaction that is interesting to be studied to understand the 511-keV line after the explosion. The rate of this reaction may influence the abundances of ^{18}F, ^{18}Ne, ^{17}F, and ^{15}O and may explain the transition sequence from the HCNO cycle to the NeNa cycle [5].

The nuclear structure of ^{18}Ne is related to the configurations and the binding energy of the levels in the mirror nucleus ^{18}O taking into account the Coulomb energies. Shell-model calculations assume a $2s$ or $1d$ nucleon coupled to the single-particle $5/2^+$, $1/2^+$, and $3/2^+$ levels of ^{17}F and ^{17}O, respectively. Comparison of the nuclear structure of the mirror nuclei for the low-lying states (2_1^+, 4_1^+, 0_2^+, 2_2^+, 2_3^+, 0_3^+, 3_1^+) shows that their excitation energies are very similar as reported in Ref. [6]. The rate of the ^{17}F(p,γ)^{18}Ne reaction has been estimated by applying several theoretical methods and experimental measurements. It is determined as a sum of the direct capture terms, including the bound states 0_1^+, 2_1^+, 4_1^+, 0_2^+, 2_2^+ and of a resonant contribution due to the states located

just above ^{17}F + p threshold, such as 1_1^-, 3_1^+, and 0_3^+ [7,8]. Wiescher, Görres, and Thielmann noticed that the $J^\pi = 3_1^+$ level in ^{18}Ne may greatly influence the thermonuclear reaction rate [9]. Recent experiments have obtained precise information about the energy of the 3_1^+ level [10,11]. Averaging their results with weights gives $E_x = 4.525(3)$ MeV, and its total width $\Gamma_p = 18(3)$ keV. Estimates of the reaction rate show that the resonant capture to the 3_1^+ state dominates the rate only at $T_9 > 0.5$ [10], which is an appropriate temperature for explosive events such as x-rays bursts and supernovae. The direct reaction measurement for ^{17}F(p,γ)^{18}Ne at ORNL determined the resonant strength. It shows that astrophysical importance of the resonant contribution is increased by a factor of 10 over the direct contribution at $T_9 = 0.5$–1.0 [12]. A slight complication occurs from the fact that ^{18}Ne is an even-Z nucleus, and its states can have more than one proton orbital involved. There are five proton bound states in ^{18}Ne and direct radiative proton capture can proceed via any and all of them. The nuclear cross section shows that the ^{17}F(p,γ)^{18}Ne reaction will be dominated by direct capture to the lowest-energy $J^\pi = 2^+$ states, mainly $E_x(2_1^+) = 1.887$ MeV and $E_x(2_2^+) = 3.616$ MeV [7].

The importance of the direct capture to the bound states in ^{18}Ne has not been resolved to date. Because of the difficulties of obtaining information from experiments with radioactive beams, we use here the asymptotic normalization coefficients (ANCs) [13] as an alternative technique to evaluate this direct capture reaction rate. The spectroscopic factors for mirror states are the same [14,15], so the ANC method can be applied to the mirror nucleus ^{18}O to extract the ANCs for the $E_x(2_1^+) = 1.982$ MeV and $E_x(2_2^+) = 3.920$ MeV states and then convert them to their corresponding states in ^{18}Ne. Measurements of ^{17}O(d,p)^{18}O [16] found that the wave functions for the $E_x(2_1^+)$ is an admixture of $(d_{5/2})^2$ and $(d_{5/2}s_{1/2})$ configurations with the spectroscopic factors 0.83 and 0.21, respectively. Similarly, the spectroscopic factors for $E_x(2_2^+)$ are 0.66 and 0.35 for the $(d_{5/2})^2$, or briefly (dd), and $(d_{5/2}s_{1/2})$, or (ds), configurations, respectively. A 25% uncertainty was estimated for these spectroscopic values [16]. The results were obtained

─────────
*abdullatq@gmail.com
†Present address: Department of Chemistry, Washington University at St. Louis, MO, USA.
‡Present address: Cooper Medical School of Rowan University, NJ, USA.

TABLE I. The parameters of the Woods-Saxon optical model potentials obtained from the analysis of the elastic-scattering data for $^{17}O + ^{13}C$ and $^{18}O + ^{12}C$.

Channel	Pot	V (MeV)	W (MeV)	r_V (fm)	r_W (fm)	a_V (fm)	a_W (fm)	χ^2	σ_R (mb)	J_V (MeV fm^3)	R_V (fm)	J_W (MeV fm^3)	R_W (fm)
$^{17}O + ^{13}C$	1	96.14	25.93	0.90	1.13	0.84	0.68	6.90	1662	215	4.64	96	4.98
	2	188.40	24.95	0.72	1.12	0.94	0.69	4.62	1667	271	4.44	92	4.99
	3	248.75	26.36	0.69	1.13	0.90	0.66	4.53	1659	318	4.27	99	4.97
$^{18}O + ^{12}C$	4	89.18	25.24	0.88	1.16	0.88	0.68	5.12	1712	197	4.69	103	5.09
	6	195.40	25.59	0.68	1.16	0.96	0.67	6.39	1702	257	4.40	104	5.07
	7	295.82	26.00	0.60	1.16	0.95	0.67	7.54	1696	297	4.20	106	5.06
	8	374.41	26.19	0.58	1.16	0.90	0.68	9.78	1695	334	4.01	107	5.07

with the aid of distorted-wave Born approximation (DWBA) calculations by fixing the geometric parameters of the Woods-Saxon potential for the radius, $r_0 = 1.25$ fm, and diffuseness, $a = 0.65$ fm.

A brief description of the experiments and the extraction of the optical potentials are presented in Sec. II. That is followed in Sec. III by the analysis of the transfer reaction data to measure the ANCs. These are finally used in model calculations to estimate and discuss the reaction rate in Sec. IV. The conclusions are summarized in Sec. V.

II. THE EXPERIMENTS

The experiments carried out were the peripheral neutron transfer reaction $^{13}C(^{17}O,^{18}O)^{12}C$ and the associated elastic scatterings in both entrance and exit channels (a rarely possible situation with nucleus-nucleus reactions). They were carried out with two separate 12 MeV/nucleon ^{17}O and ^{18}O beams from the K500 superconducting cyclotron at Texas A&M University. Each beam was transported through the beam analysis system to the scattering chamber of the multipole-dipole-multipole (MDM) magnetic spectrometer [17], where it interacted with 100-μg/cm^2 targets. The Oxford detector [18] was used in the focal plane to observe the reaction products. We have measured the neutron pickup from ^{13}C ($S_n = 4.95$ MeV) and the elastic scattering to determine the optical model parameters (OMPs) for the incoming and outgoing channels. First, the ^{17}O beam bombarded a ^{13}C target. The elastic-scattering angular distribution was measured for the spectrometer angles $4°$–$25°$ in the laboratory system. The $4° \times 1°$ wide-opening mask and an angle mask consisting of five narrow ($\Delta\theta = 0.1°$) slits were used for each spectrometer angle to double check the absolute values of the cross section and the quality of the angle calibration. Fine-tuned RAYTRACE [19] calculations were used to reconstruct the position of particles in the focal plane and the scattering angle at the target. The instrumental setup, including the focal plane detector, and the procedure for energy and angle calibrations are identical to that described in Ref. [20]. Second, the ^{12}C target was bombarded by an ^{18}O beam with 216 MeV of total laboratory energy. The elastic-scattering cross section was measured at $4°$–$22°$ spectrometer angles. The angular resolution, $\Delta\theta_{res}$, of the detector in both cases was, on average, $0.31°$ in the center-of-mass frame and the focal plane position resolution was better than 1 mm. The absolute values of cross sections

were determined using a careful integration of beam charge in a Faraday cup and the measurement of target thicknesses from energy loss of α particles from sources and from the beam. The procedures are detailed in Ref. [20] and the uncertainties are specified throughout the text.

Using reduced χ^2 as a criterion to get the best fit of the elastic-scattering data, three distinct families of potentials with standard Woods-Saxon (WS) volume form factors were obtained for $^{17}O + ^{13}C$ scattering and four sets for the $^{18}O + ^{12}C$ case. Their parameters are presented in Table I, where only central potential terms have been included (see Ref. [21] and references therein). All of the potentials give relatively small χ^2, but only those with the smallest values for entrance and exit channels, potentials 3 and 4, respectively, are adopted in the DWBA calculations of the neutron transfer reaction, while the others are used to determine the uncertainty in the choice of the OMP for either channel. The elastic-scattering fits with those potentials are plotted in Fig. 1. The pattern is characteristic for strong
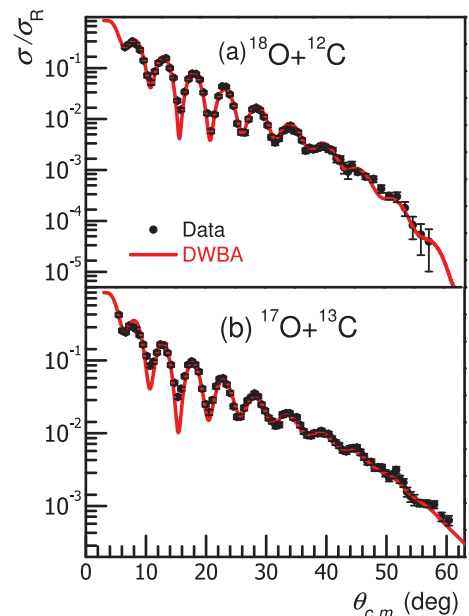

FIG. 1. (Color online) Angular distributions for the elastic-scattering data (filled circles) for (a) $^{18}O + ^{12}C$ and (b) $^{17}O + ^{13}C$ at 12 MeV/nucleon. The solid curves are calculations with the best-fit optical potentials from Table I.
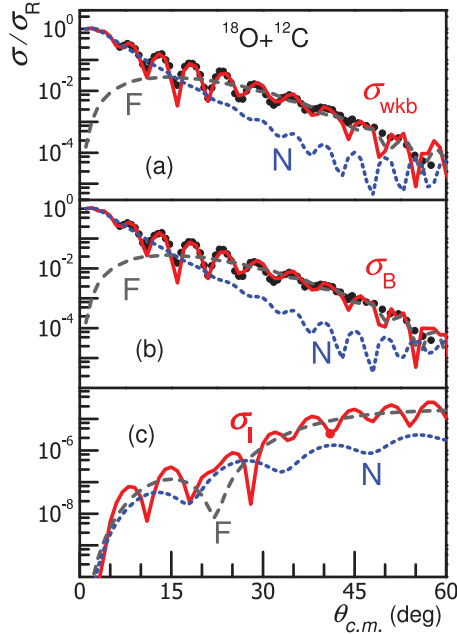
FIG. 2. (Color online) (a) Semiclassical (WKB) analysis of the cross section based on the parameter set 4, Table I. (b) The barrier (σ_B) and (c) the internal barrier (σ_I) are further decomposed into far (F) and near side (N) components, which are indicated by dashed and dotted lines, respectively.

FIG. 3. (Color online) The multi-Gaussian fit used to extract the angular distributions for the excited states in ^{18}O when the spectrometer angle is at $4°$. The solid curve represents the overlapped states beside the well-separated 2_1^+ state. The curves for the 4_1^+, 2_2^+, and the mixed state are plotted using dotted, dash-dotted, and dashed peaks, respectively. See the text for the explanation of the left most peak.

absorption with Fraunhofer oscillations at forward angles and a smoothly decaying cross section at larger angles due to far-side dominance. The peripherality of the reaction was checked by performing a detailed Wentzel-Kramers-Brillouin (WKB) analysis according to the Brink-Takigawa prescription [22]. The barrier and internal barrier component of the semiclassical scattering amplitude are shown in Fig. 2 for ^{18}O + ^{12}C. The barrier component which accounts for the flux reflected at the most external turning point of the potential fully accounts for the total cross section in the measured angular range, while the internal barrier component is negligibly small. The reaction is completely peripheral. Similar results were obtained for the case of the ^{17}O + ^{13}C elastic data at same energy $E = 12$ MeV/nucleon and are not shown explicitly here. The results of the analysis are shown in Table I.

III. ASYMPTOTIC NORMALIZATION COEFFICIENTS

The neutron transfer reaction ^{13}C(^{17}O,^{18}O)^{12}C has been measured in the laboratory frame for the spectrometer angles $4°$–$11°$, which is equivalent to $10°$–$26°$ in the center of mass. The ground state and the excited states $J^\pi = 0_1^+$, 2_1^+, 4_1^+, and 2_2^+ of ^{18}O were observed. Extracting information for the first $J^\pi = 0_1^+$ and 2_1^+ ($E = 1.982$ MeV) states is straightforward. However, due to the energy resolution of the detector, $\Delta E_{\mathrm{res}} = 350$ keV, an overlap exists between the tails of 4_1^+ ($E = 3.555$ MeV) and 2_2^+ ($E = 3.920$ MeV). Populating the 1_1^- excited state ($E^* = 4.456$ MeV) in ^{18}O and the parasitic reaction ^{13}C(^{17}O,^{18}O)^{12}C* are also present. The positions of their peaks are strongly overlapped and interfere slightly with the 2_2^+ peak. To solve the problem, RAYTRACE was used to do an
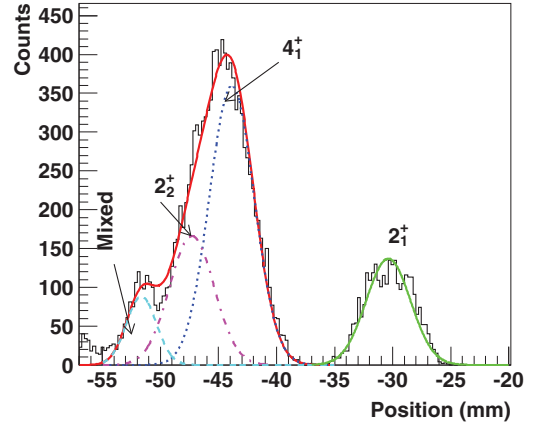
energy calibration for the first few low-lying states in ^{18}O and their expected positions along the dispersive x axis in the focal plane of the detector. Using the information about the full width at half maximum of the 2_1^+ peak and the determined positions of the other states of interest in ^{18}O, a multi-Gaussian macro was written to extract the angular distribution of the inelastic transfer reactions. Two main constraints are included in the macro, the separation between the 2_2^+ and 4_1^+ positions and the width of their corresponding peaks for each spectrometer angle, as illustrated in Fig. 3. The contribution of the 0_2^+ excited state at 3.634 MeV has been estimated. Its angular distribution was calculated and then rescaled by its relevant spectroscopic factor 0.28 reported in Ref. [16]. Comparing its cross section with those measured for 4_1^+ and 2_2^+ gives a ratio of $\frac{1}{40}$ and $\frac{1}{19}$, respectively. Including these ratios in the macro to search for 0_2^+, the fit did not show any significant change for the integration of the peaks shown in Fig 3. Therefore, the contribution of the 0_2^+ is dropped out from our determinations, but an additional uncertainty of 2.5% and 1% are added to the values of the ANCs for 4_1^+ and 2_2^+, respectively. The position spectra in the focal plane were produced from the data with the $4° \times 1°$ wide-mask with eight $0.5°$ gates on the reconstructed target angle, and the measurements at $4°$, $6°$, and $8°$ allowed a self-consistency check of the data for at least two bins.

The angular distributions for $J^\pi = 0_1^+$ and 4_1^+ are shown in Fig. 4, and those for 2_1^+ and 2_2^+ states are shown in Fig. 5. Taking into consideration the shell-model configurations [16], the ANC for each 2^+ state is determined using

$$\frac{d\sigma}{d\Omega} = \frac{C_{p_{1/2}}^2(^{13}\mathrm{C})}{b_{p_{1/2}}^2(^{13}\mathrm{C})}$$

$$\times \left\{ C_{d_{5/2}}^2(^{18}\mathrm{O}) \frac{\sigma_{d_{5/2}}^{\mathrm{DWBA}}}{b_{d_{5/2}}^2(^{18}\mathrm{O})} + C_{s_{1/2}}^2(^{18}\mathrm{O}) \frac{\sigma_{s_{1/2}}^{\mathrm{DWBA}}}{b_{s_{1/2}}^2(^{18}\mathrm{O})} \right\},$$
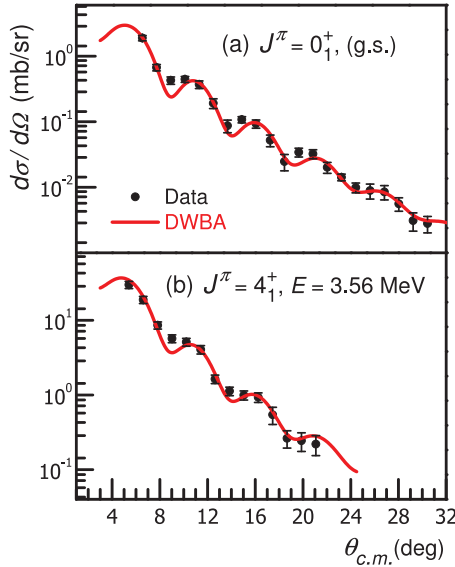
$$(1)$$

FIG. 4. (Color online) The angular distributions for populating (a) the ground state and (b) 4^+ excited state of ^{18}O. The points are the experimental data, while the solid curves are the DWBA cross sections obtained from PTOLEMY.

where $C^2_{p_{1/2}}(^{13}$C$)$ represents the ANC for the other vertex of the reaction. b_{nlj} is the single-particle ANC and its value is obtained from the ratio between the normalized single-particle bound-state neutron wave function for a specific orbital and the corresponding Hankel function at radii greater than 5.0 fm. The ANCs for the 0^+_1 and 4^+_1 states are extracted using only the
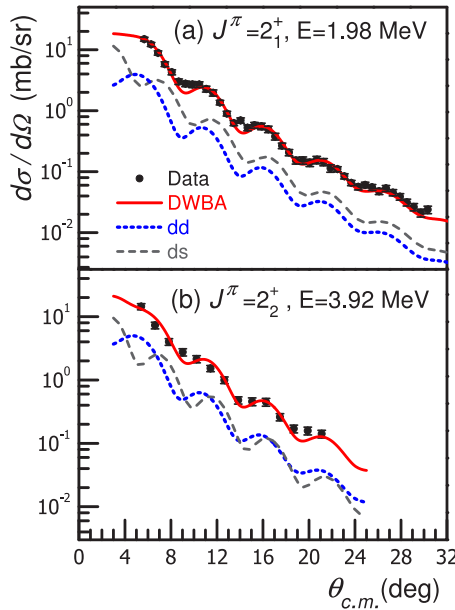

FIG. 5. (Color online) The cross section values for transfer reactions to the (a) 2^+_1 and (b) 2^+_2 states in ^{18}O. The DWBA calculations, drawn with solid curves, are the sum of the (dd) and (ds) lines. The angular distribution for the (dd) (dots) and (ds) (dashes) configurations of the 2^+ states are reduced by a factor of 5 to show their contributions.

first term of the equation. The peripherality of the reaction was checked by studying the influence of changing the geometries of the WS neutron binding potential in ^{18}O, $r_0 = 1.1$–1.3 fm and $a = 0.50$–0.65, on the ANC and spectroscopic factor values. We found that its ANC varies by less than 4% around its mean value, while its spectroscopic factor differs by more than 25%, demonstrating that only the asymptotic part of the wave function contributes in the DWBA calculations and the reaction is peripheral at 12 MeV/nucleon beam energy. The ANC of the ground state of ^{13}C, $C^2_{p_{1/2}} = 2.31 \pm 0.08$ fm^{-1}, has been found in Ref. [23]. This value is needed in Eq. (1) to extract the ANCs for the ground state and excited states in ^{18}O. The main uncertainties in the values of the ANCs for ^{17}O $+ n \rightarrow ^{18}$O are due to the (3%) in the $C^2_{p_{1/2}}(^{13}$C$)$, (7.5%) in the thickness of the target, almost (3%) statistical errors, and (4%) due to Gaussian fit for nearby states. The uncertainties in the selection of the optical potential sets for each reaction channel, and the WS geometry of the neutron binding potential used in the DWBA calculation, are not the same for all configurations, but their average values are (2.5%) and (3.5%), respectively. The total uncertainty is around 10%.

The ANCs for the 2^+_1 state were obtained by normalizing the calculated DWBA angular distributions for (dd) and (ds) configurations simultaneously to the data. Ratio of the spectroscopic factors for these $\ell = 0$ to $\ell = 2$ in the (2^+_1) state is 0.21 ± 0.03, which agrees with the measured ratio 0.22 ± 0.05 reported in Refs. [16,24]. Weighing the calculations by χ^2 gives $C^2_{d_{5/2}}(2^+) = 2.10 \pm 0.23$ fm^{-1} and $C^2_{s_{1/2}}(2^+) = 5.77 \pm 0.63$ fm^{-1}. In contrast, the ANCs for 2^+_2 were obtained by fixing the ratio between the spectroscopic factors for the (dd) and (ds) components to the measured value 0.53 ± 0.08 from Ref. [16]. Then, the normalizing procedure, using Eq. (1), was performed with one degree of freedom that is related to the (dd) configuration. This procedure added 2% and 11% to the (dd) and (ds) uncertainties, respectively. The extracted ANCs are $C^2_{d_{5/2}}(2^+_2) = 0.45 \pm 0.06$ fm^{-1} and $C^2_{s_{1/2}}(2^+_2) = 4.11 \pm 0.62$ fm^{-1}. For the 0^+_1 and 4^+_1 states we found that their (dd) spectroscopic factors are 1.50 ± 0.13 and 1.31 ± 0.14, while the measured values reported in Ref. [16] are 1.22 ± 0.31 and 1.57 ± 0.39, respectively. The ANCs for the 0^+_1 state is $C^2_{d_{5/2}}(0^+_1) = 8.18 \pm 0.76$ fm^{-1} and for the 4^+_1 is $C^2_{d_{5/2}}(4^+_1) = 1.31 \pm 0.16$ fm^{-1}.

IV. THE ^{17}F$(p, \gamma)^{18}$Ne REACTION RATE

The ANCs of the bound states in ^{18}Ne are determined from those of their corresponding states in the mirror nucleus ^{18}O using the equality of the spectroscopic factors, which leads to the relation $C^2_{nlj}(^{18}$Ne$) = [b^2_{nlj}(^{18}$Ne$)/b^2_{nlj}(^{18}$O$)]C^2_{nlj}(^{18}$O$)$. The single-particle ANC, b, in ^{18}Ne was calculated for a proton bound in a WS potential with the same geometry, $r_0 = 1.25$ fm and $a = 0.65$ fm, and the same spin-orbit interaction that were used for a neutron bound in ^{18}O. Only the depth of the central potential was adjusted to reproduce the experimental proton separation energy for each state in ^{18}Ne. The values obtained by this procedure for the depth of the nuclear potential are similar to those of the nuclear potentials found for ^{18}O. This is a very good confirmation of the charge symmetry assumption

TABLE II. The single-particle orbitals and the ANCs of the low-lying levels in ^{18}O and ^{18}Ne.

J^π	Orbital	$C^2_{\ell j}(^{18}\text{O})$ (fm^{-1})	$C^2_{\ell j}(^{18}\text{Ne})$ (fm^{-1})
0^+_1	$1d_{5/2}$	8.18 ± 0.76	12.2 ± 1.2
2^+_1	$1d_{5/2}$	2.10 ± 0.23	2.85 ± 0.32
	$2s_{1/2}$	5.77 ± 0.63	14.9 ± 2.1
4^+_1	$1d_{5/2}$	1.31 ± 0.16	2.73 ± 0.35
2^+_2	$1d_{5/2}$	0.45 ± 0.06	2.46 ± 0.33
	$2s_{1/2}$	4.11 ± 0.62	117 ± 20

made here. The ANCs obtained for the four bound states in ^{18}Ne are listed in Table II. However, using a three-body model, a symmetry breaking in mirror ANCs for ^{18}O and ^{18}Ne is estimated [25]. While this breaking is about 3% for all (dd) configurations, it can be inaccurate up to 12% for the (ds) configurations of the $2^+_{1,2}$ states. Since this variation is very large in comparison with any other calculations on mirror states, the adopted uncertainty for (ds) case is 9%. This mismatch contributes less than the uncertainties of the extracted ANCs in ^{18}Ne but it has been included.

Finally, using these nuclear structure data—the ANCs in Table II—the contributions to the astrophysical S factor for the ^{17}F(p,γ)^{18}Ne direct capture to each bound state were calculated using R-matrix approach. The proton binding WS potential was fixed using $r_0 = 1.25$ fm and $a = 0.65$ fm. Only the $E1$ electromagnetic transitions and p and f waves are considered when calculating the direct capture contributions. The S factors as a function of the center-of-mass energy for the $J^\pi = 0^+_1$, 2^+_1, 4^+_1, and 2^+_2 states of ^{18}Ne are plotted in Fig. 6, where $S(E)$ for the 2^+_1 and 2^+_2 states is the sum of their (dd) and (ds) components. It should be noted that the $(1d_{5/2}2s_{1/2})_{2^+}$ component contributes most in the proton capture. This is easy to understand due to the lack of a centrifugal barrier for the $2s_{1/2}$ orbital in the final state which extends further from the core into the asymptotic region where the proton capture happens. The figure shows that the transitions to
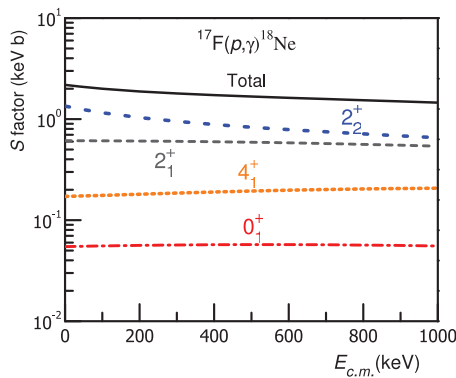

FIG. 6. (Color online) The S-factor components of the ^{17}F(p,γ)^{18}Ne reaction. $S(0)$ of the $J^\pi = 2^+_2$ state (large dotted line) makes the major contribution and is almost 50% larger than the 2^+_1 contribution (dashed line). The other components due to $J^\pi = 4^+_1$ (small dotted line) and $J^\pi = 0^+_1$ (dash-dotted line) are one order of magnitude smaller than the major one.

$J^\pi = 2^+_{1,2}$ dominate the direct capture reaction rate over the other contributions, and the $J^\pi = 2^+_2$ state makes the larger contribution at all energies. The estimated S factors at zero energy for the 0^+_1, 2^+_1, 4^+_1 and 2^+_2, are, respectively, 0.06 ± 0.01, 0.61 ± 0.11, 0.17 ± 0.03, and 1.34 ± 0.24 keV b. The variations in the S values are calculated using the ANCs' uncertainties given in Table II and the dependence of the R-matrix approach on the channel radius. The total S factor (in keV b) as a function of E (in keV) is well fit by

$$S_{1-17}(0) = 2.17 - 1.76 \times 10^{-3} E$$
$$+ 1.98 \times 10^{-6} E^2 - 9.4 \times 10^{-10} E^3. \quad (2)$$

The value of the total S factor at zero energy is $S_{1-17}(0) = 2.17 \pm 0.37$ keV b, which is 25% lower than $S(0) = 2.9 \pm 0.4$ keV b computed by García *et al.* [7]. However, there are significant differences when we compare our results with model-dependent calculations by Dufour and Descouvemont [26] and Chatterjee *et al.* [27]. Dufour used a microscopic two-cluster, two-channel generator coordinate method (GCM) with Volkov nuclear NN potential. Despite the attempt to correct the Gaussian behavior of the generator function at large intercluster distances, the usage of the Volkov potential overestimates the calculated ANCs, see Table 4 of Ref. [26], compared to our experimental ones, and sometimes quite significantly. It reflects the well-known fact that microscopically calculated ANCs are very sensitive to the choice of the NN potential, and the Volkov potential is not the best choice. Therefore, the calculated S factor due to $E1$ transition is $S(0) = 3.5$ keV b, 60% higher than ours. The other approach by Chatterjee slightly differs. The calculated ANCs in the framework of the shell model embedded in the continuum are comparable to our ANCs, except for the (ds) configuration of the 2^+_2 state which is almost two times larger. However, their $S(0)$ due to $E1$ transition is about 0.65 keV b, almost 3 times smaller than our estimate. Although Chatterjee increased the reaction rate by giving more contributions to $M1$ transition over $E1$ [27], his total S factor is still small. As a double check, we recalculated the S factor at low energies using the RADCAP code [28] and the results obtained by the R-matrix calculations were successfully reproduced.

Using the central energy of the Gamow peak for $p + {}^{17}$F, $E_o = 0.52T_9^{2/3}$ MeV, and $\tau = \frac{18.03}{T_9^{1/3}}$, the effective S factor in terms of T_9 is given by

$$S_{\text{eff}}(T_9) = 2.17\big[1 + 0.023T_9^{1/3} - 4.20 \times 10^{-4} T_9^{2/3} - 6.80$$
$$\times 10^{-5} T_9 + 2.45 \times 10^{-7} T_9^{4/3} + 1.01 \times 10^{-7} T_9^{5/3}\big],$$
$$(3)$$

TABLE III. The parameters used to calculate the resonance reaction rate.

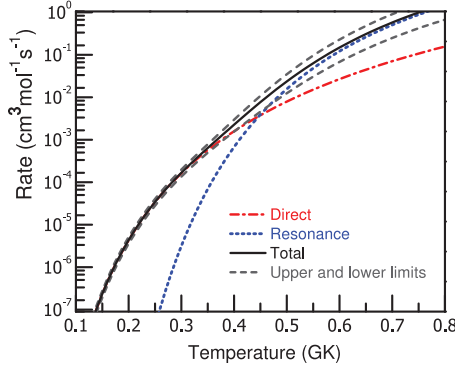| $E_{\text{c.m.}}$ (keV)	J^π	Γ_γ (meV)	$\omega\gamma$ (meV)	Ref.
597 ± 5	1^-_1	15(3)	3.8(8)	[7]
599.8 ± 2	3^+_1	56(38)	33(22)	[10,12]
665 ± 5	0^+_3	1.0(2)	0.08(2)	[7]

FIG. 7. (Color online) The direct (dash-dots) and resonant (dots) capture-rate contributions to the ^{17}F$(p,\gamma)^{18}$Ne reaction. The direct capture strongly dominates the rate for temperatures in ONe novae; $T_9 < 0.5$. The upper and lower limits of the total rate are indicated by dashed lines.

where $S_{\text{eff}}(T_9)$ is in keV b. With this equation, the estimated direct capture reaction rate for ^{17}F$(p,\gamma)^{18}$Ne is

$$N_A \langle \sigma v \rangle = 51\tau^2 S_{\text{eff}}(T_9)e^{-\tau} \left[\frac{\text{cm}^3}{\text{mole s}} \right], \qquad (4)$$

where N_A is Avogadro's number and $\langle \sigma v \rangle$ is the reaction rate per particle. The total direct capture rate has been estimated. The uncertainty in the reaction rate is dominated by the 17% overall uncertainty of the extracted ANCs. Thus, we evaluated the direct capture reaction rate of ^{17}F$(p,\gamma)^{18}$Ne through the measurement of the ANCs in the mirror nuclear system. In units of cm^3 mole^{-1} s^{-1}, the indirect capture through the resonance states given in Table III was calculated using

$$N_A \langle \sigma v \rangle_r = \frac{1.540 \times 10^{11}}{(\mu T_9)^{3/2}} \sum_i \omega\gamma_i e^{-11.605E_{R_i}/T_9}, \qquad (5)$$

where μ is the reduced mass in amu, E_{R_i} are the center-of-mass energies, and the $\omega\gamma_i$ are the strengths of the resonances in MeV. A comparison between the two rates is illustrated in Fig. 7. The present results show that the thermonuclear reaction rate is dominated by the direct capture component by one to four orders of magnitude over the resonant contribution for the relevant temperature range $T_9 = 0.2$–0.4 in ONe novae.

Our direct reaction rate is, on average, 17% lower than García's [7] calculations for temperatures less than $T_9 = 0.4$. The $\pm 17\%$ uncertainty covers the central values of the previous calculations, but it is more important because it is evaluated from measured values that provides a significant reduction in the uncertainty of the rate. In Table IV, we present the contributions from both resonant and nonresonant terms to the total reaction rate. The upper and lower limits are calculated depending on the variations extracted from measurements and their sequences are shown in Fig. 7. The resultant total rate is almost 15% lower than recent estimates by Chipps [12].

No new nucleosynthesis calculations were made here, but we can use the analysis that Parete-Koon *et al.* [29] made of the astrophysical consequences of four different rates available at the time, analysis spurned by the then recent identification of the 3_1^+ state in ^{18}Ne, the resonance considered to give the largest contribution to the resonant capture. The present new rate for the ^{17}F$(p,\gamma)^{18}$Ne reaction is slow and is very close to the ORNL rate in the direct part and identical in the resonant part. This implies that the analysis made there for the ORNL rate should hold [12]. In comparison with Bardayan [10] and Chipps [12], our rate predicts higher abundances of ^{17}O and ^{17}F in the hottest zones of 1.25 M$_\odot$ and 1.35 M$_\odot$ novae.

Although the overall uncertainty of ^{17}F$(p,\gamma)^{18}$Ne is of the order of 50%, but it is still the most important reaction to consider for its influence on the production of ^{18}F. Measuring the strength of the 665-keV resonance from ^{18}F$(p,\gamma)^{19}$Ne shows that it has almost no role in the destruction of ^{18}F within the relevant temperature regime associated with ONe novae [30]. Direct measurement of the ^{17}O$(p,\gamma)^{18}$F at Gamow energies using the two narrow resonances 66 and 183 keV gives a reduction in the synthesis of ^{18}O and ^{18}F by 10% [31].

V. CONCLUSIONS

In conclusion, we have measured the neutron transfer reaction ^{13}C$(^{17}$O,^{18}O$)^{12}$C and the elastic scattering for ^{17}O + ^{13}C and ^{18}O + ^{12}C. The OMPs (of the WS shape) were obtained to be used in DWBA analysis, as precise description of the input and exit channels of the transfer reaction. The

TABLE IV. The direct, resonant and total reaction rates in cm^3 mole^{-1} s^{-1} for ^{17}F$(p,\gamma)^{18}$Ne. The upper and lower limits were calculated including the measured uncertainties.

T_9	Direct	Resonance	Total	Upper	Lower
0.1	2.28×10^{-9}	1.19×10^{-25}	2.28×10^{-9}	2.64×10^{-9}	1.91×10^{-9}
0.2	4.35×10^{-6}	5.35×10^{-11}	4.35×10^{-6}	5.04×10^{-6}	3.65×10^{-6}
0.3	1.64×10^{-4}	3.16×10^{-6}	1.67×10^{-4}	1.95×10^{-4}	1.39×10^{-4}
0.4	1.59×10^{-3}	6.77×10^{-4}	2.27×10^{-3}	2.94×10^{-3}	1.59×10^{-3}
0.5	7.92×10^{-3}	1.57×10^{-2}	2.36×10^{-2}	3.47×10^{-2}	1.26×10^{-2}
0.6	2.68×10^{-2}	1.21×10^{-1}	1.48×10^{-1}	2.28×10^{-1}	6.84×10^{-2}
0.7	7.06×10^{-2}	5.05×10^{-1}	5.76×10^{-1}	9.02×10^{-1}	2.50×10^{-1}
0.8	1.57×10^{-1}	1.43×10^{0}	1.59×10^{0}	2.51×10^{0}	6.73×10^{-1}
0.9	3.06×10^{-1}	3.16×10^{0}	3.46×10^{0}	5.48×10^{0}	1.45×10^{0}
1.0	5.44×10^{-1}	5.84×10^{0}	6.39×10^{0}	1.01×10^{1}	2.66×10^{0}

peripherality of the reaction mechanism was studied using a semiclassical method and from proving that the ANCs are independent of the geometries of the neutron-binding potential. The ANCs of the bound states of ^{18}O were extracted and transposed to their mirror states in ^{18}Ne to determine the S factor for the ^{17}F(p,γ)^{18}Ne reaction. We found that its reaction rate is dominated by direct capture to the 2_1^+ and 2_2^+ states in ^{18}Ne. As far as we know, this is the first time the direct capture reaction using measured ANCs has been evaluated. Our rate is slow and implies more production of ^{18}F in 1.25 M$_\odot$ novae. Direct measurements, if possible using (probably) ^{17}F radioactive nuclear beams in inverse kinematics, may clarify the importance of direct capture for the rate of the ^{17}F(p,γ)^{18}Ne reaction rate in novae. Indirect methods measurements like the Coulomb or nuclear breakup of ^{18}Ne may give some useful information for its ground state (ANC) and be compared with the one extracted here using its ^{18}O mirror.

[1] J. Gómez-Gomar, M. Hernanz, J. José, and J. Isern, Mon. Not. R. Astron. Soc. **296**, 913 (1998).

[2] M. J. Harris, J. E. Naya, B. J. Teegarden, T. L. Cline, N. Gehrels, D. M. Palmer, R. Ramaty, and H. Seifert, Astrophys. J. **522**, 424 (1999).

[3] J. José, M. Hernanz, and C. Iliadis, Nucl. Phys. A **777**, 550 (2006).

[4] A. Coc, M. Hernanz, J. José, and J. Thibaud, Astron. Astrophys. **357**, 561 (2000).

[5] R. K. Wallace and S. E. Woosley, Astrophys. J. Suppl. Ser. **45**, 389 (1981).

[6] R. Sherr and H. T. Fortune, Phys. Rev. C **58**, 3292 (1998).

[7] A. García, E. G. Adelberger, P. V. Magnus, D. M. Markoff, K. B. Swartz, M. S. Smith, K. I. Hahn, N. Bateman, and P. D. Parker, Phys. Rev. C **43**, 2012 (1991).

[8] K. I. Hahn, A. García, E. G. Adelberger, P. V. Magnus, A. D. Bacher, N. Bateman, G. P. A. Berg, J. C. Blackmon, A. E. Champagne, B. Davis et al., Phys. Rev. C **54**, 1999 (1996).

[9] M. Wiescher, J. Görres, and F.-K. Thielemann, Astrophys. J. **326**, 384 (1988).

[10] D. W. Bardayan, J. C. Blackmon, C. R. Brune, A. E. Champagne, A. A. Chen, J. M. Cox, T. Davinson, V. Y. Hansper, M. A. Hofstee, B. A. Johnson et al., Phys. Rev. Lett. **83**, 45 (1999).

[11] Y. Parpottas, S. M. Grimes, S. Al-Quraishi, C. R. Brune, T. N. Massey, J. E. O'Donnell, J. E. Oldendick, A. Salas, and R. T. Wheeler, Phys. Rev. C **72**, 025802 (2005).

[12] K. A. Chipps, D. W. Bardayan, J. C. Blackmon, K. Y. Chae, U. Greife, R. Hatarik, R. L. Kozub, C. Matei, B. H. Moazen, C. D. Nesaraja et al., Phys. Rev. Lett. **102**, 152502 (2009).

[13] H. M. Xu, C. A. Gagliardi, R. E. Tribble, A. M. Mukhamedzhanov, and N. K. Timofeyuk, Phys. Rev. Lett. **73**, 2027 (1994).

[14] L. Trache, A. Azhari, F. Carstoiu, H. L. Clark, C. A. Gagliardi, Y.-W. Lui, A. M. Mukhamedzhanov, X. Tang, N. Timofeyuk, and R. E. Tribble, Phys. Rev. C **67**, 062801(R) (2003).

[15] N. K. Timofeyuk, R. C. Johnson, and A. M. Mukhamedzhanov, Phys. Rev. Lett. **91**, 232501 (2003).

[16] T. K. Li, D. Dehnhard, R. E. Brown, and P. J. Ellis, Phys. Rev. C **13**, 55 (1976).

[17] D. M. Pringle, W. N. Catford, J. S. Winfield, D. G. Lewis, N. A. Jelley, K. W. Allen, and J. H. Coupland, Nucl. Instrum. Methods A **245**, 230 (1986).

[18] J. S. Winfield, D. M. Pringle, W. N. Catford, D. G. Lewis, N. A. Jelley, and K. W. Allen, Nucl. Instrum. Methods A **251**, 297 (1986).

[19] S. Kowalski and H. A. Enge, computer code raytrace (unpublished), University of Oxford, England, UK, 1986.

[20] A. M. Mukhamedzhanov, V. Burjan, F. Carstoiu, J. Cejpek, H. L. Clark, C. A. Gagliardi, Y.-W. Lui, V. Kroha, L. Trache, R. E. Tribble et al., Phys. Rev. C **56**, 1302 (1997).

[21] F. Carstoiu, L. Trache, R. E. Tribble, and C. A. Gagliardi, Phys. Rev. C **70**, 054610 (2004).

[22] D. M. Brink and N. Takigawa, Nucl. Phys. A **279**, 159 (1977).

[23] T. Al-Abdullah, F. Carstoiu, X. Chen, H. L. Clark, C. Fu, C. A. Gagliardi, Y.-W. Lui, A. Mukhamedzhanov, G. Tabacaru, Y. Tokimoto et al., Phys. Rev. C **81**, 035802 (2010).

[24] R. L. Lawson, F. J. D. Serduke, and H. T. Fortune, Phys. Rev. C **14**, 1245 (1976).

[25] N. K. Timofeyuk and I. J. Thompson, Phys. Rev. C **78**, 054322 (2008).

[26] M. Dufour and P. Descouvemont, Nucl. Phys. A **730**, 316 (2004).

[27] R. Chatterjee, J. Okołowicz, and M. Płoszajczak, Nucl. Phys. A **764**, 528 (2006).

[28] C. A. Bertulani, Comput. Phys. Commun. **156**, 123 (2003).

[29] S. Parete-Koon, W. R. Hix, M. S. Smith, S. Starrfield, D. W. Bardayan, M. W. Guidry, and A. Mezzacappa, Astrophys. J. **598**, 1239 (2003).

[30] C. Akers, A. M. Laird, B. R. Fulton, C. Ruiz, D. W. Bardayan, L. Buchmann, G. Christian, B. Davids, L. Erikson, J. Fallis et al., Phys. Rev. Lett. **110**, 262502 (2013).

[31] D. A. Scott, A. Caciolli, A. D. Leva, A. Formicola, M. Aliotta, M. Anders, D. Bemmerer, C. Broggini, M. Campeggio, P. Corvisiero et al., Phys. Rev. Lett. **109**, 202501 (2012).